THE JOURNAL OF PHYSICAL CHEMISTRY B
A JOURNAL OF THE AMERICAN CHEMICAL SOCIETY

pubs.acs.org/JPCB

Article

Quantifying Species Populations in Multivalent Borohydride Electrolytes

Nathan T. Hahn,* Julian Self, Kee Sung Han, Vijayakumar Murugesan, Karl T. Mueller, Kristin A. Persson, and Kevin R. Zavadil

Cite This: https://doi.org/10.1021/acs.jpcb.1c00263

Read Online

ACCESS | Metrics & More | Article Recommendations | Supporting Information

ABSTRACT: Multivalent batteries represent an important beyond Li-ion energy storage concept. The prospect of calcium batteries, in particular, has emerged recently due to novel electrolyte demonstrations, especially that of a ground-breaking combination of the borohydride salt $Ca(BH_4)_2$ dissolved in tetrahydrofuran. Recent analysis of magnesium and calcium versions of this electrolyte led to the identification of divergent speciation pathways for Mg^{2+} and Ca^{2+} despite identical anions and solvents, owing to differences in cation size and attendant flexibility of coordination. To test these proposed speciation equilibria and develop a more quantitative understanding thereof, we have applied pulsed-field-gradient nuclear magnetic resonance and dielectric relaxation spectroscopy to study these electrolytes. Concentration-dependent variation in anion diffusivities and solution dipole relaxations, interpreted with the aid of molecular dynamics simulations, confirms these divergent Mg^{2+} and Ca^{2+} speciation pathways. These results provide a more quantitative description of the electroactive species populations. We find that these species are present in relatively small quantities, even in the highly active $Ca(BH_4)_2$/tetrahydrofuran electrolyte. This finding helps interpret previous characterizations of metal deposition efficiency and morphology control and thus provides important fundamental insight into the dynamic properties of multivalent electrolytes for next-generation batteries.

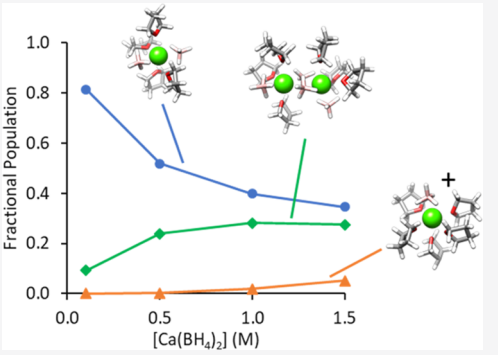

INTRODUCTION

Li-ion batteries have come to dominate the global portable electronics and electrified vehicle markets, but further advances in batteries are required to meet anticipated energy storage needs for a diversity of applications.[1] Among the proposed avenues toward this goal, multivalent batteries, including Ca, Mg, Zn, and Al, are intriguing options due to the high energy densities and generally lower reactivities of their metallic anodes compared to Li.[2] The alkaline earth chemistries of Mg and Ca have received growing interest recently due to their significantly negative redox potentials, yielding the prospect of high cell voltage.[2−4] These high voltages, however, come at the cost of electrolyte stability, which must be managed to maintain high efficiencies and rates for the corresponding metal plating and stripping reactions. Because of this requirement, early-stage electrolyte demonstrations have largely originated from exotic formulations containing chemically reducing salts including organometallics facilitated by chloride dissolved in ethereal solvents such as tetrahydrofuran (THF).[5,6] One of the first nonhalide magnesium salts demonstrated to reversibly deposit Mg was $Mg(BH_4)_2$,[7,8] and the first such calcium salt to function in this manner at room temperature was $Ca(BH_4)_2$.[9] The ground-breaking nature of these electrolytes highlights the importance of the borohydride class as a system of fundamental study, despite its obvious drawbacks from the standpoint of oxidative reactivity. Moreover, understanding the links between borohydride solvation environments and properties has high potential impact on both solid-state electrolytes and reversible hydrogen storage, areas in which borohydrides are under active investigation.[10−13]

While several investigations into the liquid solvation environment of $Mg(BH_4)_2$ electrolytes have been conducted,[7,8,14−17] understanding of $Ca(BH_4)_2$ electrolyte solvation is relatively nascent.[18,19] Our recent findings underscored the importance of BH_4^- coordination in determining speciation and delivery of the metal cation to the interface.[19] The most probable ionic species determined from density-functional theory (DFT) calculations were found to be $CaBH_4^+$ and $Ca(BH_4)_3^-$, indicating that the electroactive species is the cationic cluster $CaBH_4^+$. Difficulty in forming the active species, whether in $Ca(BH_4)_2$/THF at low salt concentrations (≤0.5 M) or in $Mg(BH_4)_2$/THF across all

Received: January 11, 2021
Revised: March 4, 2021

salt concentrations, reduces the measured metal deposition current density and Coulombic efficiency.[19] These findings also implicated the role of multimer formation in facilitating the creation of these important ionic species based on X-ray absorption spectroscopy, a key feature differentiating the behavior of the Mg and Ca electrolytes based on their configurational flexibility differences. The term "configurational flexibility" reflects the fact that Ca^{2+} can adopt a wider range of bonding configurations due to its greater size and polarizability than Mg^{2+}.[20,21] To validate these proposed speciation details from a more quantitative perspective, we report complimentary investigation into $Mg(BH_4)_2$ and $Ca(BH_4)_2$ solutions in THF via pulsed-field-gradient nuclear magnetic resonance (PFG-NMR) and dielectric relaxation spectroscopy (DRS). The results of this investigation confirm a significantly greater population of electroactive ionic species in the Ca system, which is particularly enhanced at high salt concentrations. By using molecular dynamics (MD) simulations to interpret the DRS data, we are able to provide a quantitative estimation of the primary species populations in solution. We demonstrate the dominance of neutral monomers in $Mg(BH_4)_2$/THF across the full concentration range and the enhancement of neutral dimers and ionic species in $Ca(BH_4)_2$/THF at high salt concentrations. Despite the enhancement of electroactive $CaBH_4^+$ at high concentrations in the Ca case, the relative population of this species is still only a small fraction of the total Ca^{2+} inventory. This fact has important ramifications for sustaining high rate and energy-efficient calcium plating from this electrolyte.

METHODS

Electrolyte Preparation. Electrolyte synthesis was performed inside a catalyst-purified, argon-filled glovebox (MBraun) with typical water and oxygen levels below 1 and 0.1 ppm, respectively. THF was purchased from Sigma-Aldrich, distilled over sodium, and stored over activated alumina and 3A molecular sieves prior to use, yielding measured water levels below 10 ppm. $Ca(BH_4)_2$·2THF, $Mg(BH_4)_2$ (95%), and $LiBH_4$ (95%) salts were purchased from Sigma-Aldrich and used as received. Ionic conductivities were measured using electrochemical impedance spectroscopy in a custom cell consisting of parallel Pt electrodes, the cell constant of which was determined using aqueous KCl solutions.

PFG-NMR. D_{anion} and $D_{solvent}$ were determined simultaneously by ^{1}H PFG-NMR using a bipolar gradient PFG sequence at 25 °C on a 600 MHz NMR spectrometer (Agilent) equipped with a 5 mm z-gradient probe (Doty Scientific). The PFG-echo profiles were obtained as a function of the gradient strength (g) with a gradient length (δ) and a diffusion delay fixed at 2 and 30 ms, respectively. The gradient strength was gradually increased in 16 equal steps to the maximum applied gradient strength to observe the full decay in the echo profiles. The recorded echo profiles, $S(g)$, were fitted with the Stejskal–Tanner equation[22]

$$S(g) = S(0)\exp\left[-D(\gamma g\delta)^2\left(\Delta - \frac{\delta}{3}\right)\right] \quad (1)$$

where $S(0)$ is the echo intensity at a gradient strength of zero. D, γ, δ, and Δ are the diffusion coefficient, the gyromagnetic ratio ($\gamma(^1H) = 2\pi\cdot 42.577$ rad·MHz·T^{-1}), the gradient length, and the time interval between the two bipolar gradient pairs, respectively. ^{43}Ca and ^{25}Mg PFG-NMR were not successful for the determination of D_{cation} for Ca^{2+} and Mg^{2+} in these solutions due to the fast nuclear relaxation rates for ^{43}Ca and ^{25}Mg in these samples.

Dielectric Relaxation Spectroscopy. DRS was performed on electrolytes in glass vials using a dielectric probe kit (Keysight N1501A) and vector network analyzer (Keysight 9375A) over a frequency range of 0.5–26.5 GHz. Each set of measurements were performed with a three-point calibration using air, a shorting block, and THF. Duplicate measurements were performed after recalibration to ensure consistency. Simultaneous fitting of the real (ε') and imaginary (ε'') components of the complex, frequency-dependent relative permittivity (eq 2) was performed numerically by deconvolution of the individual dipole relaxation processes (eq 3).[23]

$$\varepsilon(\nu) = \varepsilon'(\nu) - i\varepsilon''(\nu) \quad (2)$$

$$\varepsilon(\nu) = \varepsilon_\infty + \sum_{j=1}^{n} \varepsilon_j[1 - (i2\pi\nu\tau_j)^{1-\alpha_j}]^{-1} \quad (3)$$

In eq 3, ε_∞ accounts for the total intramolecular polarizability of the solution, while the n solution dipole reorientation contributions are included in the summation term based on each dipole's permittivity amplitude (ε), relaxation time (τ), and broadening or Cole–Cole parameter (α). For Debye relaxations, $\alpha = 0$. Ionic conductivities (used to extract ε'' from the permittivity data) measured by impedance spectroscopy were treated as fixed parameters during the fitting process. It was determined that the spectra obtained from the $Mg(BH_4)_2$/THF solutions were best fit by one Debye relaxation for the solvent and one Cole–Cole relaxation for the salt, while the spectra from $Ca(BH_4)_2$/THF solutions were best fit by two to three Debye relaxations. Summation of these relaxation amplitudes yields the total dielectric constant, ε_t, of the solution (see the Supporting Information for fitting parameters, Tables S1 and S2). The 1.0 M $Mg(BH_4)_2$ solution was observed to react at the probe tip, nucleating small bubbles, which impacted the measured parameters. The data reported for this system were thus averaged over completely independent electrolyte makeups and calibrations (see the Supporting Information, Table S2). The conclusions are not impacted by the uncertainty in this data point. Aside from the 1.0 M $Mg(BH_4)_2$ solution, the samples showed consistent dielectric constants in repeated measurements (typically better than ±0.05). Species populations were determined by combining the measured dielectric constant changes with calculated dielectric increments ($\Delta\varepsilon$) and $\Lambda/\Lambda_{NMR,eff}$ measurements, as described in the Supporting Information document.

Computational Simulations. Dielectric increment calculations were performed using classical MD simulations, as discussed in previous publications.[24,25] Single salt species (such as contact ion pairs, etc.) were placed in a box with 112 THF solvent molecules (approx. 0.10–0.11 M) using PACKMOL. With GROMACS MD software, these electrolytes were equilibrated first using a Berendsen barostat (NPT), followed by heating and cooling steps. Afterward, production runs in the NVT using the velocity rescaling thermostat were undertaken. In these regimes, salt species were associated for the duration of the simulation (each at least 10 ns), and from their dipole moment, in addition to the dipole moment of the solvent species, the dielectric constant of the entire electrolyte solution was found. The dielectric constant of the neat THF solution was subtracted from this value, which was then subsequently

https://doi.org/10.1021/acs.jpcb.1c00263
J. Phys. Chem. B XXXX, XXX, XXX–XXX

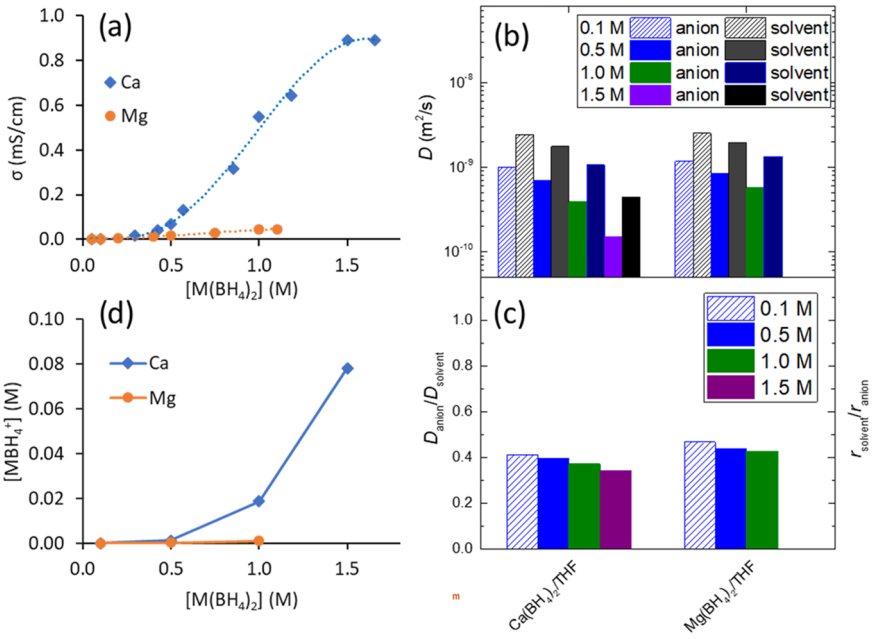

Figure 1. (a) Ionic conductivity values measured for $Mg(BH_4)_2$ and $Ca(BH_4)_2$ in THF as a function of concentration (adapted from ref 19 with permission from the Royal Society of Chemistry). Dotted lines represent polynomial fits serving as guides to the eye. (b) Diffusivity values of BH_4^- and THF measured by PFG-NMR as a function of the borohydride salt concentration. (c) Relative diffusivities of anion to solvent calculated from the PFG-NMR data. (d) Calculated concentrations of $CaBH_4^+$ and $MgBH_4^+$ in the solution as a function of the overall salt concentration based on an effective ionicity ratio analysis, assuming ionic species of MBH_4^+ and $M(BH_4)_3^-$.

divided by the concentration (e.g., 0.11 M) to obtain the dielectric increment per salt species, as appearing in the Supporting Information (Tables S3 and S4, Figure S4). For associated salt species with an overall charge, the overall charge was subtracted from the dipole moment, as discussed in a previous publication.[24] The force field parameter files for BH_4^- were the same as those from Rajput et al.,[19,26] the THF force field files from Caleman et al., and the Ca and Mg force field files from the standard OPLS force field.[27,28] Error estimates appearing in Tables S3 and S4 were calculated from duplicate simulations and analyses.

RESULTS AND DISCUSSION

An increase in relative electroactive ionic species populations with the overall salt concentration is demonstrated in that the ionic conductivities of both $Mg(BH_4)_2$/THF and $Ca(BH_4)_2$/THF solutions increase with concentration despite a drop in the average BH_4^- diffusivity. Although the conductivity increase is much more dramatic for $Ca(BH_4)_2$ than for $Mg(BH_4)_2$, both increase significantly on a relative basis (Figure 1a). When the conductivity values are normalized by concentration yielding molar conductivities, Λ, the positive trends persist up to 1 M (Supporting Information, Figure S1). An increase in Λ should represent an increase either in the ionicity (relative formation of ionic species) of the electrolyte or in the diffusivities of the ionic species. Since the PFG-NMR-measured diffusivity of BH_4^-, (D_{anion}) decreases by nearly a factor of 2 in both solutions as the concentration increases from 0.1 to 1.0 M (Figure 1b), the dominant factor must be an ionicity increase. This increase is clearly enhanced in the Ca system.

The significant ionicity increase in these solutions occurs despite their strong ion-pairing tendencies. The presence of extensive ion pairing is demonstrated by the relative anion and solvent diffusivities as measured by PFG-NMR. As shown in Figure 1b, the decrease in D_{anion} is accompanied by a decrease in THF diffusivity ($D_{solvent}$) with increasing concentration. This can be attributed to both an increase in the solution viscosity (η) and an increased fraction of THF bound to the metal cations. To account for the solution viscosity changes, the ratio of $D_{anion}/D_{solvent}$ was calculated in each case (Figure 1c). Viscosity should affect both anion and solvent diffusivities in a similar manner based on the Stokes−Einstein relation $D \sim (\eta R)^{-1}$, where R is the effective radius of the solution species. In all solutions, D_{anion} is less than half of $D_{solvent}$, despite the fact that the calculated radius of gyration (R_g) of BH_4^- from MD simulations (R_g = 0.6 Å) is smaller than that of THF (R_g = 1.4 Å). This difference in R_g means that a "free" BH_4^- anion should diffuse much faster than a free THF molecule. The fact that $D_{anion} < D_{solvent}$ indicates that most, if not all, of the BH_4^- anions are coordinated to metal cations, forming clusters with significantly larger effective radii than free BH_4^- and yielding a lower average D_{anion} value. Indeed, the calculated R_g values for associated clusters from MD simulations are between 2.5 and 4.5 Å, i.e., approximately twice as large as the R_g of THF. This size difference is generally consistent with the measured $D_{anion}/D_{solvent}$ values (Supporting Information, Tables S3 and S4).

The absence of free BH_4^- is consistent with previously reported Raman measurements that were unable to detect free BH_4^- in these electrolytes and with DFT calculations showing that dissociation of BH_4^- from Ca^{2+} or Mg^{2+} is unfavorable.[15,19] Indeed, even the dissociation of BH_4^- from Li^+ is highly unfavorable in THF.[29] Furthermore, DFT calculations indicated that the primary ionic species in $Ca(BH_4)_2$/THF are most likely the associated clusters $CaBH_4^+$ and $Ca(BH_4)_3^-$, in which case the overall equilibrium could be considered as

$$2Ca(BH_4)_2 \leftrightarrow CaBH_4^+ + Ca(BH_4)_3^- \quad (4)$$

The differences in measured Λ between the Ca^{2+} and Mg^{2+} electrolytes imply that these clusters form much more readily

https://doi.org/10.1021/acs.jpcb.1c00263
J. Phys. Chem. B XXXX, XXX, XXX−XXX

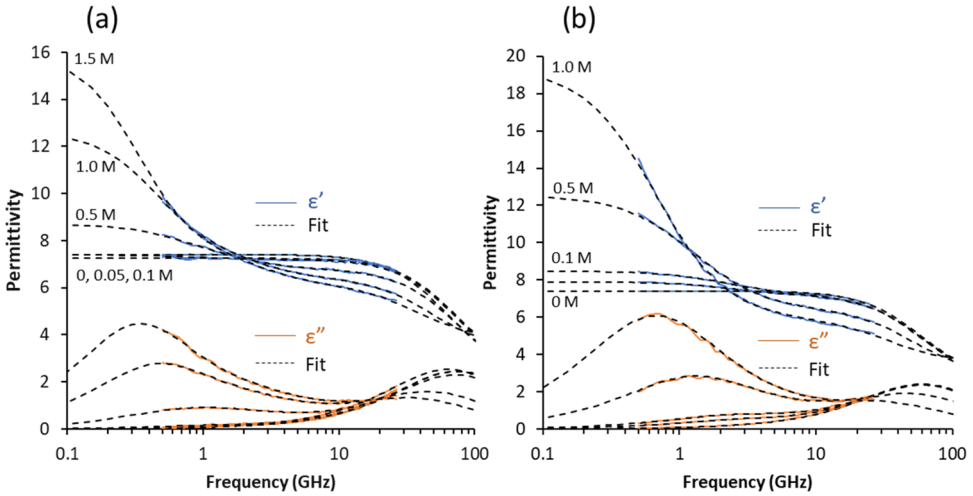

Figure 2. Real (ε', top) and imaginary (ε'', bottom) components of the complex permittivity measured as a function of frequency in (a) $Ca(BH_4)_2$/THF and (b) $Mg(BH_4)$/THF. Solid lines represent the measured data, while dashed lines represent fits of the data based on a summation of Debye and/or Cole−Cole relaxations. Deconvolutions of these relaxations are shown in the Supporting Information, Figure S2.

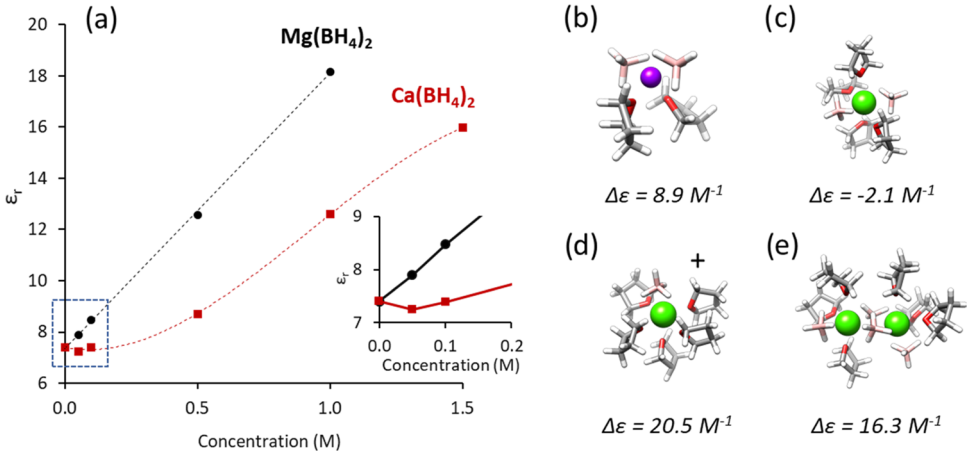

Figure 3. (a) Solution dielectric constants (ε_r) determined from fits of the complex permittivity data as a function of concentration. Dotted lines represent trend lines for the ε_r vs concentration data (linear in the case of Mg^{2+} and polynomial in the case of Ca^{2+}). Inset: magnification of the plots at low concentrations. (b−e) Representative cluster structures to which the ε_r changes are attributed. The calculated net dielectric increment ($\Delta\varepsilon$) of each cluster is indicated. These species are referred to as (b) Mg neutral monomer, (c) Ca neutral monomer, (d) Ca CIP (contact ion pair) cation, and (e) Ca neutral dimer (bent configuration). Mg, Ca, B, C, H, and O atoms are shown in purple, green, pink, gray, white, and red, respectively. The calculated parameters and uncertainties of all species investigated are shown in Tables S3 and S4 in the Supporting Information.

from $Ca(BH_4)_2$ than from $Mg(BH_4)_2$ in THF. The fact that $D_{anion}/D_{solvent}$ decreases with increasing concentration in both $Ca(BH_4)_2$ and $Mg(BH_4)_2$ solutions confirms that enhanced populations of free BH_4^- (which would increase $D_{anion}/D_{solvent}$) are not the origin of the increase in ionicity. If anything, this trend implies that some degree of salt aggregation is favored at high concentrations in both solutions, although previous work indicated that $Ca(BH_4)_2$ more readily forms multimeric species than $Mg(BH_4)_2$ in THF.[19,30−33] These results validate our hypothesis that the primary origin of the increasing Λ vs concentration trend in alkaline earth borohydride solutions is the enhanced formation of associated ionic clusters such as MBH_4^+ rather than the liberation of free BH_4^- or a possible increase in ion diffusivity.[34]

Considering these results in light of the proposed ionic species (MBH_4^+ and $M(BH_4)_3^-$),[19] we estimate their concentrations from the measured Λ and D_{anion} values based on an effective ionicity ratio $\Lambda/\Lambda_{NMR,eff}$ (i.e., effective Haven ratio), where $\Lambda_{NMR,eff}$ is the molar conductivity expected if all of the dissolved salt is converted into the proposed ionic species. This value is given by eq 5[35]

$$\Lambda_{NMR,eff} = \frac{eF}{k_B T}\left(\frac{D_i z_i^2 c_i}{c_{salt}} + \frac{D_j z_j^2 c_j}{c_{salt}}\right) \quad (5)$$

In eq 5, species i and j refer to MBH_4^+ and $M(BH_4)_3^-$, respectively, D is the species self-diffusion coefficient, z is the species charge, c is the species concentration, and c_{salt} is the overall salt concentration. Therefore, $z_i = z_j = 1$ and $c_i/c_{salt} = c_j/c_{salt} = 0.5$ based on stoichiometry. To a first approximation, it is assumed that $D_i = D_j$, i.e., $D(MBH_4^+) = D(M(BH_4)_3^-)$, and that these diffusivities are approximately equal to the ensemble-measured anion (BH_4^-) diffusivity. These assumptions are based on the lack of free BH_4^- and on the similarity of the calculated R_g values for the resulting metal borohydride clusters in MD simulations (Supporting Information, Tables S3 and S4). Furthermore, the charged cluster diffusivities are not expected to differ much from those of the neutral

https://doi.org/10.1021/acs.jpcb.1c00263
J. Phys. Chem. B XXXX, XXX, XXX−XXX

clusters.[36,37] The contributions of the charged clusters to $\Lambda_{NMR,eff}$ are approximated as ideal, i.e., long-range interionic interactions are neglected. Thus, ionic populations estimated from the effective ionicity may be somewhat underestimated. The MBH_4^+ concentrations resulting from this analysis are shown in Figure 1d. These calculations highlight the remarkable increase in the concentration of these electroactive species as a function of the overall salt concentration in the Ca system. These species are almost nonexistent at salt concentrations less than 0.5 M, which readily explains the severely inhibited Ca electrodeposition response reported at such concentrations.[19] Since the Mg system possesses very low concentrations of $MgBH_4^+$ at all salt concentrations, its metal deposition response is inhibited even at high salt concentrations. This is consistent with previous reports demonstrating that alkali-salt additives ($LiBH_4$ or $NaBH_4$) are required to achieve adequate Mg electrodeposition rate and reversibility.[7,15,16,38]

Significant differences in the concentration-dependent speciation pathways of the Mg and Ca electrolytes are manifested in the complex permittivity responses of the solvated species. DRS spectra measured across a range of salt concentrations in these two systems reveal their characteristic frequency-dependent permittivity (Figure 2). In both systems, two primary relaxations are observed: a high-frequency solvent relaxation ($f \sim 30$ to 70 GHz) and a low-frequency relaxation corresponding to dipolar salt clusters ($f \sim 0.3-3$ GHz). The relaxation frequencies of the $Ca(BH_4)_2$ salt clusters are somewhat lower than those of $Mg(BH_4)_2$, presumably due to the larger size of Ca^{2+} and its related complexes. In $Ca(BH_4)_2$/THF, the impact of dipolar salt clusters on the solution permittivity is not significant until salt concentration exceeds 0.1 M, while in $Mg(BH_4)_2$/THF, these clusters are significant even at 0.05 M. Due to the presence of these clusters, the dielectric constants (ε_r) of the concentrated solutions are far greater than that of the neat THF solvent ($\varepsilon_r = 7.4$), reaching values as high as 18.2 for $Mg(BH_4)_2$ and 16.0 for $Ca(BH_4)_2$ (Figure 3a). Our observation of a net increase in ε_r is consistent with previous investigations of strongly associating alkali salts in low permittivity solvents.[24,39−41] Recently, we speculated that ε_r could increase to a value as high as 10 in $Ca(BH_4)_2$/THF due to such effects,[19] but this value turns out to have been a significant underestimation. The most important difference in the permittivity behavior of the Mg and Ca systems lies in the functional forms of the ε_r vs concentration dependence (Figure 3a). In $Mg(BH_4)_2$/THF, ε_r increases linearly across the entire concentration range, while in $Ca(BH_4)_2$/THF, the ε_r change is nonlinear and even nonmonotonic. The linear $Mg(BH_4)_2$ behavior implies an essentially static speciation profile in which one or more dipolar clusters are present at a constant relative population regardless of salt concentration. In contrast, the $Ca(BH_4)_2$ behavior implies an evolving speciation profile where the relative dipolar cluster populations vary significantly with salt concentration. This result speaks to the configurational flexibility differences of Ca^{2+} and Mg^{2+}.[19−21]

Our previous investigations led us to conclude that the primary solvated species in $Mg(BH_4)_2$/THF is the neutral, monomeric form of the dissolved salt across all concentrations, based on the low measured conductivities and the reported tendency of $Mg(BH_4)_2$ toward forming monomeric solvates.[19,31,32] To test whether such species could explain the linear and steeply sloped ε_r vs concentration trend, the dielectric increments ($\Delta\varepsilon$) of several clusters were simulated by MD; the parameter $\Delta\varepsilon$ represents the net change in ε_r that a given cluster would induce when formed in a THF medium at a concentration of 1 M. The neutral monomer, $Mg(BH_4)_2$, possesses a highly asymmetric structure and a large dipole moment leading to a large computed net $\Delta\varepsilon$ of 8.9 M^{-1}. This value agrees well with the net $\Delta\varepsilon$ of 9.4 M^{-1} measured for this electrolyte across the entire concentration range (Supporting Information, Figure S3). This agreement suggests that these neutral monomers are the majority solvated species across this concentration range. We note that the small populations of $MgBH_4^+$ species predicted from conductivity and diffusivity analyses are unlikely to be observed by DRS due to their low concentration. For comparison, measurements of $LiBH_4$/THF as a simpler 1:1 salt system ostensibly dominated by neutral contact ion pairs (CIPs) in THF ($K_A \sim 10^9$)[29] also yielded a linear ε_r vs concentration trend (Supporting Information, Figure S4). As in the Mg case, the $\Delta\varepsilon$ derived from the $LiBH_4$ measurements agrees with the calculated $\Delta\varepsilon$ value (9.2 vs 9.7). This agreement between the measured overall $\Delta\varepsilon$ and calculated neutral monomer $\Delta\varepsilon$ in both systems provides strong evidence that both systems are dominated by these species at the concentrations investigated. In previous studies, salt clusters composed of a single cation and two anions ("triple ions") were sometimes presumed as linear and thus not detectable as dipolar species by DRS.[40,42] However, a more rigorous evaluation of cluster dielectric increments by MD simulations clearly shows that such structural assumptions can be misleading, as exemplified by the case of $Mg(BH_4)_2$/THF.

In $Ca(BH_4)_2$/THF, we recently proposed that neutral monomers ($Ca(BH_4)_2$) are prevalent at low salt concentrations and that these are progressively converted to multimeric and ionic species such as $Ca_2(BH_4)_4$, $CaBH_4^+$, and $Ca(BH_4)_3^-$ as salt concentration is increased.[19] Calculations of these species' $\Delta\varepsilon$ values indicate that our hypothesized trajectory of species evolution can explain the unique ε_r vs concentration trend measured in this system (Figure 3). MD simulations reveal that the neutral calcium monomer is much more symmetric than the magnesium analogue and has almost no dipole moment (Figure 3c), resulting in a $\Delta\varepsilon$ of -2.1 M^{-1}. The negative $\Delta\varepsilon$ arises from the fact that several THF molecules are bound to this solvated cluster and can no longer contribute to the background dielectric constant. Therefore, a population of solvated neutral monomers can readily explain the small initial decrease in the measured dielectric constant of ~0.1 units at 0.05 M (Figure 3a, inset). At concentrations above 0.1 M, the measured dielectric constant increases significantly above that of neat THF, signaling a shift in the solution equilibria toward more polar clusters.

Analysis of the hypothesized clusters reveals that both $CaBH_4^+$ ($\Delta\varepsilon = 20.5$ M^{-1}) and $Ca_2(BH_4)_4$ ($\Delta\varepsilon = 16.3$ M^{-1}) could contribute significantly to the permittivity increase measured in $Ca(BH_4)_2$/THF. The large dielectric increment of the dimer species is surprising given that neutral dimers are often assumed to have negligible dipole moments due to their approximately symmetric structure.[40,43] However, over our simulated MD trajectory, we find that this $Ca_2(BH_4)_4$ cluster frequently rearranges into bent or pyramidal configurations, leading to a significant time-averaged dipole moment magnitude and a resulting dielectric increment of 16.3 M^{-1} (Supporting Information, Figure S5). This again highlights the importance of MD simulations in accurately accounting for the range of conformations that a given cluster may adopt. The

https://doi.org/10.1021/acs.jpcb.1c00263
J. Phys. Chem. B XXXX, XXX, XXX−XXX

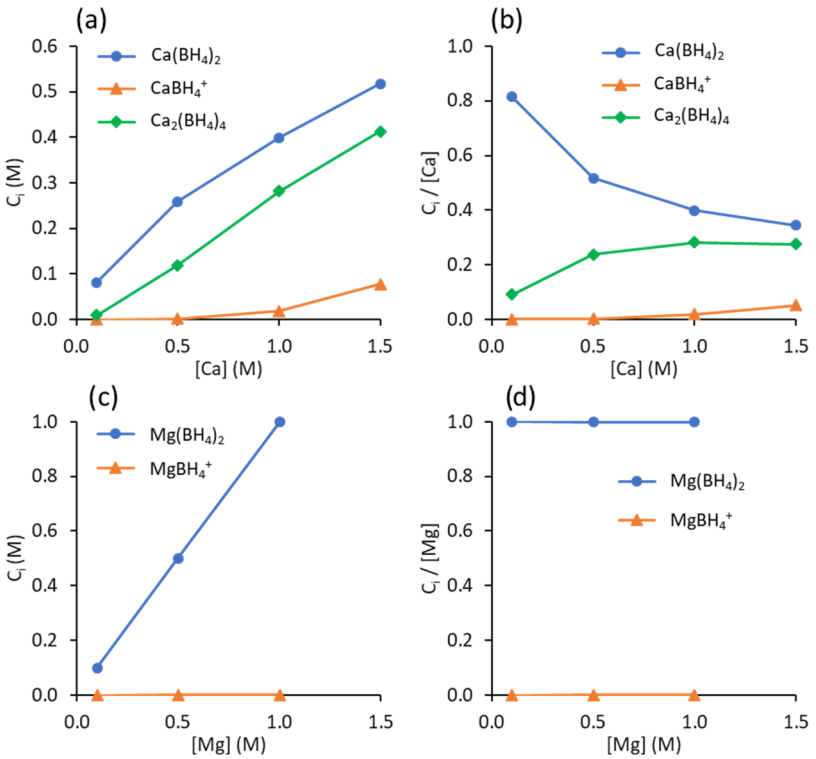

Figure 4. Concentrations of the major solvated species calculated from the effective ionicity analysis combined with DRS measurements and modeling as a function of the overall salt concentration for (a, b) $Ca(BH_4)_2$/THF and (c, d) $Mg(BH_4)_2$/THF. The data are plotted either (a, c) as species concentrations or (b, d) as relative populations. It is assumed that $[MBH_4^+] = [M(BH_4)_3^-]$.

calculated $\Delta\varepsilon$ values allow for estimation of various species populations contributing to the overall measured $\Delta\varepsilon$, assuming an equilibrium distribution among the four proposed major species

$$2Ca(BH_4)_2 \leftrightarrow Ca_2(BH_4)_4 \leftrightarrow CaBH_4^+ + Ca(BH_4)_3^- \quad (6)$$

The MD-simulated $\Delta\varepsilon$ values of these species were used to calculate the self-consistent populations that could account for the measured overall $\Delta\varepsilon$ at each salt concentration. To bolster this approach, the calculations were refined by incorporating the $CaBH_4^+$ and $Ca(BH_4)_3^-$ concentrations predicted from the aforementioned effective ionicity analysis (as shown in Figure 1d). Without this input, the species populations cannot be inferred precisely due to difficulties in differentiating the contributions of $CaBH_4^+$ and $Ca_2(BH_4)_4$ to ε_r (Supporting Information, Figure S6). The calculated speciation diagrams (Figure 4a,b) reveal that the neutral monomer is the dominant species at low salt concentrations of 0.1 M and below, that these species are partially converted to dimers at moderate to high salt concentrations, and that small populations of the ionic species become stabilized at high salt concentrations. In $Mg(BH_4)_2$/THF, however, the neutral monomers are more strongly favored and almost no change in speciation is observed (Figure 4c,d).

The fact that dimers account for at least half of the total calcium inventory in $Ca(BH_4)_2$/THF solutions at high salt concentrations ensures their detection via X-ray absorption spectroscopy,[19] lending credence to these calculations. The high concentration of polar dimers and the resulting solution permittivity increase likely help stabilize the ionic clusters. This phenomenon is analogous to the "redissociation" mechanism proposed in previous investigations.[24,40,44] However, this term usually refers to the facilitation of free ion formation, whereas in our case, the increase in conductivity is caused by ionic cluster formation. To the best of our knowledge, this is the first time that the stabilization of ionic clusters rather than free ions has been attributed to the accumulation of polar salt species. It is surprising that this stabilization mechanism does not operate as effectively in $Mg(BH_4)_2$/THF despite its high concentration of polar monomers and larger relative increase in dielectric constant. We speculate that this is due to a smaller thermodynamic equilibrium constant for forming the necessary ionic clusters, i.e., $MgBH_4^+$ and $Mg(BH_4)_3^-$, due to the greater charge density and lesser polarizability of Mg^{2+}. Therefore, the configurational flexibility of Ca^{2+} remains an important criterion for the effective ionic cluster formation in these strongly ion-associating solutions.

Although the proposed electroactive species $CaBH_4^+$ constitutes only a minority population in $Ca(BH_4)_2$/THF, the kinetics of species interconversion likely prevent $CaBH_4^+$ from becoming selectively depleted at the anode surface during calcium plating (i.e., cell charging). The kinetics of ion pairing and dissociation are generally fast enough, by many orders of magnitude,[45] to prevent species-specific depletion due to electrochemical consumption at an electrode, provided the overall concentration of salt is maintained. However, the concentration-dependent thermodynamics of speciation, as inferred from Figure 4, predict a strong suppression of $[CaBH_4^+]$ near the surface and in the diffusion layer if large salt concentration gradients are formed during high rate and/or high-capacity calcium plating. This suppression of ionic species may lead to a significant Ohmic potential drop despite high bulk salt concentrations. Moreover, low concentrations of electroactive $CaBH_4^+$ near the electrode may promote parasitic reactions and loss of calcium morphology control. Indeed, a

https://doi.org/10.1021/acs.jpcb.1c00263
J. Phys. Chem. B XXXX, XXX, XXX−XXX

recent study highlighted that such rate-dependent calcium plating problems are encountered in $Ca(BH_4)_2$/THF electrolytes.[46] Therefore, we propose the relatively small, concentration-dependent population of $CaBH_4^+$ as the underlying cause. Our findings thus inform both recent and ongoing efforts at studying interfacial phenomena in these unique electrolyte environments.

CONCLUSIONS

Complimentary analyses of ionic conductivity, anion diffusivity, and solution permittivity provide a quantitative understanding of solvation in an important class of alkaline earth metal borohydride electrolytes in THF. The primary findings of these analyses are (1) both $Mg(BH_4)_2$ and $Ca(BH_4)_2$ electrolytes exhibit an increase in ionicity with concentration despite extensive ion pairing in both systems; (2) electroactive MBH_4^+ species populations are much more favored in the latter case, especially at high salt concentrations; (3) $Mg(BH_4)_2$/THF is dominated by neutral monomers across the full concentration range, while $Ca(BH_4)_2$/THF speciation evolves from neutral monomers to multimers and ionic species; and (4) the population of the electroactive $CaBH_4^+$ species in $Ca(BH_4)_2$/THF is less than 0.1 M, even in high-salt-concentration electrolytes (1−1.5 M) that support high Coulombic efficiency electrodeposition. The ability to quantify species populations in the $Ca(BH_4)_2$/THF electrolyte represents an important contribution to the understanding of these systems that directly links to recent demonstrations of surface and interfacial phenomena.

ASSOCIATED CONTENT

Supporting Information

The Supporting Information is available free of charge at https://pubs.acs.org/doi/10.1021/acs.jpcb.1c00263.

Ionic conductivity measurements, DRS methods, DRS fitting examples, DRS extracted parameters, cluster calculations, and speciation diagrams (PDF)

AUTHOR INFORMATION

Corresponding Author

Nathan T. Hahn − *Joint Center for Energy Storage Research, Lemont, Illinois 60439, United States; Material, Physical and Chemical Sciences Center, Sandia National Laboratories, Albuquerque, New Mexico 87185, United States;* orcid.org/0000-0001-6187-4068; Email: nthahn@sandia.gov

Authors

Julian Self − *Joint Center for Energy Storage Research, Lemont, Illinois 60439, United States; Department of Materials Science and Engineering, University of California, Berkeley, California 94720, United States; Energy Technologies Area, Lawrence Berkeley National Laboratory, Berkeley, California 94720, United States;* orcid.org/0000-0002-5486-9559

Kee Sung Han − *Joint Center for Energy Storage Research, Lemont, Illinois 60439, United States; Physical and Computational Sciences Directorate, Pacific Northwest National Laboratory, Richland, Washington 99354, United States;* orcid.org/0000-0002-3535-1818

Vijayakumar Murugesan − *Joint Center for Energy Storage Research, Lemont, Illinois 60439, United States; Physical and Computational Sciences Directorate, Pacific Northwest National Laboratory, Richland, Washington 99354, United States;* orcid.org/0000-0001-6149-1702

Karl T. Mueller − *Joint Center for Energy Storage Research, Lemont, Illinois 60439, United States; Physical and Computational Sciences Directorate, Pacific Northwest National Laboratory, Richland, Washington 99354, United States;* orcid.org/0000-0001-9609-9516

Kristin A. Persson − *Joint Center for Energy Storage Research, Lemont, Illinois 60439, United States; Department of Materials Science and Engineering, University of California, Berkeley, California 94720, United States; The Molecular Foundry, Lawrence Berkeley National Laboratory, Berkeley, California 94720, United States;* orcid.org/0000-0003-2495-5509

Kevin R. Zavadil − *Joint Center for Energy Storage Research, Lemont, Illinois 60439, United States; Material, Physical and Chemical Sciences Center, Sandia National Laboratories, Albuquerque, New Mexico 87185, United States;* orcid.org/0000-0002-3791-424X

Complete contact information is available at: https://pubs.acs.org/10.1021/acs.jpcb.1c00263

Notes

The authors declare no competing financial interest.

ACKNOWLEDGMENTS

This work was supported by the Joint Center for Energy Storage Research, an Energy Innovation Hub funded by the U.S. Department of Energy. Sandia National Laboratories is a multimission laboratory managed and operated by the National Technology & Engineering Solutions of Sandia, LLC, a wholly owned subsidiary of Honeywell International Inc., for the U.S. Department of Energy's National Nuclear Security Administration under contract DE-NA0003525. This research used resources of the National Energy Research Scientific Computing Center, a DOE Office of Science User Facility supported by the Office of Science of the U.S. Department of Energy under contract no. DE-AC02-05CH11231. The PFG-NMR measurements were performed at the Environmental Molecular Sciences Laboratory (EMSL), a national scientific user facility sponsored by the DOE's Office of Biological and Environmental Research and located at Pacific Northwest National Laboratory (PNNL). This paper describes objective technical results and analysis. Any subjective views or opinions that might be expressed in the paper do not necessarily represent the views of the U.S. Department of Energy or the United States Government.

REFERENCES

(1) Trahey, L.; Brushett, F. R.; Balsara, N. P.; Ceder, G.; Cheng, L.; Chiang, Y.-M.; Hahn, N. T.; Ingram, B. J.; Minteer, S. D.; Moore, J. S.; et al. Energy storage emerging: A perspective from the joint center for energy storage research. *Proc. Natl. Acad. Sci. U.S.A.* **2020**, *117*, 12550−12557.

(2) Liang, Y.; Dong, H.; Aurbach, D.; Yao, Y. Current status and future directions of multivalent metal-ion batteries. *Nat. Energy* **2020**, *5*, 646−656.

(3) Ponrouch, A.; Frontera, C.; Bardé, F.; Palacín, M. R. Towards a calcium-based rechargeable battery. *Nat. Mater.* **2016**, *15*, 169−172.

(4) Arroyo-de Dompablo, M. E.; Ponrouch, A.; Johansson, P.; Palacín, M. R. Achievements, challenges, and prospects of calcium batteries. *Chem. Rev.* **2020**, *120*, 6331−6357.

(5) Mizrahi, O.; Amir, N.; Pollak, E.; Chusid, O.; Marks, V.; Gottlieb, H.; Larush, L.; Zinigrad, E.; Aurbach, D. Electrolyte

solutions with a wide electrochemical window for rechargeable magnesium batteries. *J. Electrochem. Soc.* **2008**, *155*, A103−A109.
(6) Viestfrid, Y.; Levi, M. D.; Gofer, Y.; Aurbach, D. Microelectrode studies of reversible mg deposition in thf solutions containing complexes of alkylaluminum chlorides and dialkylmagnesium. *J. Electroanal. Chem.* **2005**, *576*, 183−195.
(7) Mohtadi, R.; Matsui, M.; Arthur, T. S.; Hwang, S.-J. Magnesium borohydride: From hydrogen storage to magnesium battery. *Angew. Chem., Int. Ed.* **2012**, *51*, 9780−9783.
(8) Shao, Y.; Liu, T.; Li, G.; Gu, M.; Nie, Z.; Engelhard, M.; Xiao, J.; Lv, D.; Wang, C.; Zhang, J.-G.; et al. Coordination chemistry in magnesium battery electrolytes: How ligands affect their performance. *Sci. Rep.* **2013**, *3*, No. 3130.
(9) Wang, D.; Gao, X.; Chen, Y.; Jin, L.; Kuss, C.; Bruce, P. G. Plating and stripping calcium in an organic electrolyte. *Nat. Mater.* **2018**, *17*, 16−20.
(10) Lu, Z.; Ciucci, F. Metal borohydrides as electrolytes for solid-state Li, Na, Mg, and Ca batteries: A first-principles study. *Chem. Mater.* **2017**, *29*, 9308−9319.
(11) Cuan, J.; Zhou, Y.; Zhou, T.; Ling, S.; Rui, K.; Guo, Z.; Liu, H.; Yu, X. Borohydride-scaffolded Li/Na/Mg fast ionic conductors for promising solid-state electrolytes. *Adv. Mater.* **2019**, *31*, No. 1803533.
(12) He, T.; Cao, H.; Chen, P. Complex hydrides for energy storage, conversion, and utilization. *Adv. Mater.* **2019**, *31*, No. 1902757.
(13) Schneemann, A.; Wan, L. F.; Lipton, A. S.; Liu, Y.-S.; Snider, J. L.; Baker, A. A.; Sugar, J. D.; Spataru, C. D.; Guo, J.; Autrey, T. S.; et al. Nanoconfinement of molecular magnesium borohydride captured in a bipyridine-functionalized metal−organic framework. *ACS Nano* **2020**, *14*, 10294−10304.
(14) Samuel, D.; Steinhauser, C.; Smith, J. G.; Kaufman, A.; Radin, M. D.; Naruse, J.; Hiramatsu, H.; Siegel, D. J. Ion pairing and diffusion in magnesium electrolytes based on magnesium borohydride. *ACS Appl. Mater. Interfaces* **2017**, *9*, 43755−43766.
(15) Deetz, J. D.; Cao, F.; Wang, Q.; Sun, H. Exploring the liquid structure and ion formation in magnesium borohydride electrolyte using density functional theory. *J. Electrochem. Soc.* **2018**, *165*, A61−A70.
(16) Deetz, J. D.; Cao, F.; Sun, H. Exploring the synergy of LiBH4/NaBH4 additives with mg(bh4)2 electrolyte using density functional theory. *J. Electrochem. Soc.* **2018**, *165*, A2451−A2457.
(17) Arthur, T. S.; Glans, P.-A.; Singh, N.; Tutusaus, O.; Nie, K.; Liu, Y.-S.; Mizuno, F.; Guo, J.; Alsem, D. H.; Salmon, N. J.; et al. Interfacial insight from operando XAS/TEM for magnesium metal deposition with borohydride electrolytes. *Chem. Mater.* **2017**, *29*, 7183−7188.
(18) Ta, K.; Zhang, R. X.; Shin, M.; Rooney, R. T.; Neumann, E. K.; Gewirth, A. A. Understanding Caa electrodeposition and speciation processes in nonaqueous electrolytes for next-generation Caa-ion batteries. *ACS Appl. Mater. Interfaces* **2019**, *11*, 21536−21542.
(19) Hahn, N. T.; Self, J.; Seguin, T. J.; Driscoll, D. M.; Rodriguez, M. A.; Balasubramanian, M.; Persson, K. A.; Zavadil, K. R. The critical role of configurational flexibility in facilitating reversible reactive metal deposition from borohydride solutions. *J. Mater. Chem. A* **2020**, *8*, 7235−7244.
(20) Katz, A. K.; Glusker, J. P.; Beebe, S. A.; Bock, C. W. Calcium ion coordination: A comparison with that of beryllium, magnesium, and zinc. *J. Am. Chem. Soc.* **1996**, *118*, 5752−5763.
(21) Carafoli, E.; Krebs, J. Why calcium? How calcium became the best communicator. *J. Biol. Chem.* **2016**, *291*, 20849−20857.
(22) Stejskal, E. O.; Tanner, J. E. Spin diffusion measurements: Spin echoes in the presence of a time-dependent field gradient. *J. Chem. Phys.* **1965**, *42*, 288−292.
(23) Buchner, R.; Hefter, G. Interactions and dynamics in electrolyte solutions by dielectric spectroscopy. *Phys. Chem. Chem. Phys.* **2009**, *11*, 8984−8999.
(24) Self, J.; Hahn, N. T.; Fong, K. D.; McClary, S. A.; Zavadil, K. R.; Persson, K. A. Ion pairing and redissociaton in low-permittivity electrolytes for multivalent battery applications. *J. Phys. Chem. Lett.* **2020**, *11*, 2046−2052.
(25) Self, J.; Wood, B. M.; Rajput, N. N.; Persson, K. A. The interplay between salt association and the dielectric properties of low permittivity electrolytes: The case of LiPF6 and LiAsF6 in dimethyl carbonate. *J. Phys. Chem. C* **2018**, *122*, 1990−1994.
(26) Rajput, N. N.; Qu, X. H.; Sa, N.; Burrell, A. K.; Persson, K. A. The coupling between stability and ion pair formation in magnesium electrolytes from first-principles quantum mechanics and classical molecular dynamics. *J. Am. Chem. Soc.* **2015**, *137*, 3411−3420.
(27) Jorgensen, W. L.; Maxwell, D. S.; Tirado-Rives, J. Development and testing of the OPLS all-atom force field on conformational energetics and properties of organic liquids. *J. Am. Chem. Soc.* **1996**, *118*, 11225−11236.
(28) Caleman, C.; van Maaren, P. J.; Hong, M.; Hub, J. S.; Costa, L. T.; van der Spoel, D. Force field benchmark of organic liquids: Density, enthalpy of vaporization, heat capacities, surface tension, isothermal compressibility, volumetric expansion coefficient, and dielectric constant. *J. Chem. Theory Comput.* **2012**, *8*, 61−74.
(29) Ashby, E. C.; Dobbs, F. R.; Hopkins, H. P. Composition of complex aluminum hydrides and borohydrides, as inferred from conductance, molecular association, and spectroscopic studies. *J. Am. Chem. Soc.* **1973**, *95*, 2823−2829.
(30) Bremer, M.; Nöth, H.; Thomann, M.; Schmidt, M. Preparation and molecular structures of tetrahydrofuran, diethylene diglycol dimethyl ether and 18-crown-6 complexes of strontium and barium tetrahydridoborate. *Chem. Ber.* **1995**, *128*, 455−460.
(31) Bremer, M.; Nöth, H.; Warchhold, M. The structure of some amine solvates of magnesium bis(tetrahydroborate) and DFT calculations on solvates of lithium tetrahydroborate. *Eur. J. Inorg. Chem.* **2003**, *2003*, 111−119.
(32) Lobkovskii, E. B.; Titov, L. V.; Psikha, S. B.; Antipin, M. Y.; Struchkov, Y. T. X-ray crystallographic investigation of crystals of bis(tetrahydroborato)tris(tetrahydrofuranato)magnesium. *J. Struct. Chem.* **1983**, *23*, 644−646.
(33) Lobkovskii, E. B.; Chekhlov, A. N.; Levicheva, M. D.; Titov, L. V. Crystal and molecular structure of the complex of calcium borohydride with diethylene glycol diethyl ether. *Khoord. Khim.* **1988**, *14*, 543−550.
(34) Petrowsky, M.; Frech, R.; Suarez, S. N.; Jayakody, J. R. P.; Greenbaum, S. Investigation of fundamental transport properties and thermodynamics in diglyme−salt solutions. *J. Phys. Chem. B* **2006**, *110*, 23012−23021.
(35) Takeuchi, M.; Kameda, Y.; Umebayashi, Y.; Ogawa, S.; Sonoda, T.; Ishiguro, S.-i.; Fujita, M.; Sano, M. Ion−ion interactions of LiPF6 and LiBF4 in propylene carbonate solutions. *J. Mol. Liq.* **2009**, *148*, 99−108.
(36) Cohen, L. H.; Saraf, D. N.; Witherspoon, P. A. Diffusion coefficients of hydrocarbons in water: Method for measuring. *Science* **1963**, *142*, 955−956.
(37) Hall, J. R.; Wishaw, B. F.; Stokes, R. H. The diffusion coefficients of calcium chloride and ammonium chloride in concentrated aqueous solutions at 25°. *J. Am. Chem. Soc.* **1953**, *75*, 1556−1560.
(38) Chang, J.; Haasch, R. T.; Kim, J.; Spila, T.; Braun, P. V.; Gewirth, A. A.; Nuzzo, R. G. Synergetic role of Li+ during Mg electrodeposition/dissolution in borohydride diglyme electrolyte solution: Voltammetric stripping behaviors on a Pt microelectrode indicative of Mg−Li alloying and facilitated dissolution. *ACS Appl. Mater. Interfaces* **2015**, *7*, 2494−2502.
(39) Delsignore, M.; Farber, H.; Petrucci, S. Ionic conductivity and microwave dielectric relaxation of lithium hexafluoroarsenate (LiAsF6) and lithium perchlorate (LiClO4) in dimethyl carbonate. *J. Phys. Chem. A* **1985**, *89*, 4968−4973.
(40) Petrucci, S.; Masiker, M. C.; Eyring, E. M. The possible presence of triple ions in electrolyte solutions of low dielectric permittivity. *J. Solution Chem.* **2008**, *37*, 1031−1035.
(41) Saar, D.; Brauner, J.; Farber, H.; Petrucci, S. Dielectric relaxation of some 1:1 electrolytes in tetrahydrofuran and diethyl carbonate. *J. Phys. Chem. B* **1978**, *82*, 1943−1947.

https://doi.org/10.1021/acs.jpcb.1c00263
J. Phys. Chem. B XXXX, XXX, XXX−XXX

(42) Buchner, R.; Chen, T.; Hefter, G. Complexity in "simple" electrolyte solutions: Ion pairing in MgSO4(aq). *J. Phys. Chem. B* **2004**, *108*, 2365−2375.
(43) Borodin, O.; Douglas, R.; Smith, G.; Eyring, E. M.; Petrucci, S. Microwave dielectric relaxation, electrical conductance, and ultrasonic relaxation of LiPF6 in poly(ethylene oxide) dimethyl ether-500. *J. Phys. Chem. B* **2002**, *106*, 2140−2145.
(44) Cavell, E. A. S.; Knight, P. C. Effect of concentration changes on permittivity of electrolyte solutions. *Z. Phys. Chem.* **1968**, *57*, 331−334.
(45) Buchner, R.; Barthel, J. Kinetic processes in the liquid phase studied by high-frequency permittivity measurements. *J. Mol. Liq.* **1995**, *63*, 55−75.
(46) Pu, S. D.; Gong, C.; Gao, X.; Ning, Z.; Yang, S.; Marie, J.-J.; Liu, B.; House, R. A.; Hartley, G. O.; Luo, J.; et al. Current-density-dependent electroplating in Ca electrolytes: From globules to dendrites. *ACS Energy Lett.* **2020**, *5*, 2283−2290.

https://doi.org/10.1021/acs.jpcb.1c00263
J. Phys. Chem. B XXXX, XXX, XXX−XXX